RESEARCH ARTICLE | MARCH 21 2024

Embedding gold nanoparticles in the SnO_2 electron transport layer for boosting flexible perovskite solar cells with the efficiency over 23%

Caoyu Long ; Erming Feng ; Jianhui Chang; Yang Ding; Yuanji Gao ; Hengyue Li ; Biao Liu ; Zijian Zheng ; Liming Ding ; Junliang Yang

Appl. Phys. Lett. 124, 123908 (2024)
https://doi.org/10.1063/5.0188072

Applied Physics Letters ARTICLE pubs.aip.org/aip/apl

Embedding gold nanoparticles in the SnO_2 electron transport layer for boosting flexible perovskite solar cells with the efficiency over 23%

Cite as: Appl. Phys. Lett. **124**, 123908 (2024); doi: 10.1063/5.0188072
Submitted: 18 November 2023 · Accepted: 11 March 2024 ·
Published Online: 21 March 2024

Caoyu Long,[1] Erming Feng,[1] Jianhui Chang,[1] Yang Ding,[1] Yuanji Gao,[1] Hengyue Li,[1,a)] Biao Liu,[1] Zijian Zheng,[2] Liming Ding,[3] and Junliang Yang[1,4,a)]

AFFILIATIONS

[1]Hunan Key Laboratory for Super-microstructure and Ultrafast Process, School of Physics, Central South University, Changsha 410083, China
[2]Department of Applied Biology and Chemical Technology, Faculty of Science, The Hong Kong Polytechnic University, Hong Kong 999077, China
[3]Center for Excellence in Nanoscience, Key Laboratory of Nanosystem and Hierarchical Fabrication (CAS), National Center for Nanoscience and Technology, Beijing 100190, China
[4]State Key Laboratory of Powder Metallurgy, Central South University, Changsha 410083, China

[a)]**Authors to whom correspondence should be addressed:** hengyueli@csu.edu.cn and junliang.yang@csu.edu.cn.
Tel.: +86-731-88660256

ABSTRACT

Flexible perovskite solar cells (*f*-PSCs) exhibit superior potential applications in space energy, mobile energy, portable energy due to the characteristics of cost-effective large-scale processing, high efficiency, and power-to-weight. It is significant to improve the electron extraction and transport in the electron transport layer (ETL) to enhance the power conversion efficiency (PCE) of *f*-PSCs. Herein, we report a highly efficient SnO_2 ETL embedded by gold nanoparticles (Au NPs) that obviously boost the PCE of *f*-PSCs. The high-conductivity Au NPs can improve the electrical properties of ETL by enhancing the conductivity and electron mobilities, which dramatically promote the electron extraction and transport, resulting in the decrease in charge recombination at the ETL/perovskite interface. An impressive PCE of 23.08% can be achieved for the *f*-PSCs with SnO_2 ETL embedded Au NPs, which is much higher than the reference *f*-PSCs with the PCE of 21.65% utilizing pristine SnO_2 ETL. This work presents an innovative approach for the fabrication of high-efficiency *f*-PSCs, which is compatible with the roll-to-roll manufacturing process.

Perovskite solar cells (PSCs) exhibit the advantages of high efficiency, low cost, and low-temperature solution processibility,[1,2] and the power conversion efficiency (PCE) of single-junction PSCs has already reached 26.1%,[3] revealing bright prospects for the commercialization. Furthermore, the soft and lightweight natures of these materials facilitate the realization of flexible PSCs (*f*-PSCs). With the tremendous efforts in the perovskite composition, interfacial engineering, and crystalline regulation, the PCE of *f*-PSCs has soared to 24.5% and 15.5% for small-area device (0.08 cm^2) and large-area modules (100 cm^2), respectively.[4–9] Recently, numerous reports have emerged regarding the efficiency of *f*-PSCs exceeding 23%. For example, Han *et al.* successfully incorporated a ferroelectric 2D material into 3D perovskite to enhance built-in electric field and precisely control the crystallization process of perovskite. As a result, they ultimately achieved *f*-PSCs with an efficiency of 23%.[4] Yi and co-workers proposed a multifunctional organic salt incorporation to alleviate strain and reinforce grain boundaries, thereby improving the long-term stability and efficiency of *f*-PSCs up to 23.6%.[5] Zhu and co-workers enhanced the PCE of *f*-PSCs to 23.68% by modifying the interface using pentylammonium acetate molecules.[6] Additionally, Li and co-workers adjusted the composition distribution within perovskite films by integrating a cross-linker, 4,5–(3-methyloxetane) dicarboxylate imidazole (MZ), resulting in f-PSCs with a remarkable PCE of 23.94% and enhanced stability.[7] Furthermore, Chen *et al.* not only mitigated defects but also alleviated residual strain by introducing a new self-healing elastomer. Notably, this elastomer effectively repaired

mechanical cracks induced by bending in the perovskite film, leading to *f*-PSCs with a PCE of 23.84% and improved stability.[8] Most recently, *f*-PSCs achieved a PCE of 24.5% using a multifunctional cross-linkable elastomer as an efficient passivation and self-healing agent, pointing toward a promising future for *f*-PSCs.[9]

It has been established that the electron transport layer (ETL) plays a crucial role in determining the efficiency, stability, and reliability of PSCs.[10] For the ETL material, SnO_2 is extensively employed due to its excellent opto-electronic property, including low-temperature process, appropriate energy band level, and high electron mobility.[11,12] However, pristine SnO_2 ETL normally exhibits unsatisfactory performance because of the enhanced defect density, inadequate crystallinity, and low conductivity for low-temperature processed SnO_2 film.[13] Especially, the mobility and conductivity of SnO_2 ETL are still inferior owing to its relatively low carrier concentration, accordingly cutting down the device performance.[14,15] Normally, the conductivity of ETL can be enhanced through structural modifications or doping strategies.[14–18] Nevertheless, tuning the structure, such as reducing the thickness or engineering with mesoporous layer, might compromise the electron blocking capability and deteriorate recombination.[17] However, the doping probably leads to phase segregation, worse morphology, intensified recombination centers, and extra absorption, thus diminishing the transport properties and compromising the light utilization.[18] Therefore, it is imperative to explore alternative approaches to optimize the SnO_2 ETL and overcome the aforementioned disadvantages.

Gold nanoparticles (Au NPs) are recommended to improve the performance parameters of solar cells by enhancing the light absorption induced by localized surface plasmon resonance (LSPR),[19–22] or regulating the charge transport, exciton dissociation, and crystallinity of perovskite layer via inserting Au NPs ultra-thin layer between the charge transport layer and the active layer.[23–26] Previous reports have primarily focused on incorporating the Au-NPs into TiO_2, NiO_x, ZnO, Spiro-OMeTAD, or perovskite active layer.[23–26] However, it remains unclear whether Au-NPs can effectively improve the charge transfer performance of SnO_2 or corresponding photovoltaic (PV) performance. Herein, we demonstrate a straightforward strategy to improve the charge transport and transfer performance of SnO_2 ETL by incorporating Au NPs into SnO_2 to form a SnO_2-Au ETL thin film. It is found that Au NPs could greatly enhance the electron mobility, conductivity, and charge transfer capability of SnO_2 ETL. However, Au NPs do not have any disadvantage effect on the morphology and crystallization of SnO_2 and perovskite films, as well as no sacrifice on the transmittance of the ETL due to low doping concentration. As a result, the *f*-PSCs with SnO_2-Au ETL exhibit an optimized PCE of 23.08%. The results provide a significant inspiration for processing highly efficient *f*-PSCs by embedding Au NPs.

The optical properties, surface morphology, chemical composition, and crystal structure on the SnO_2 ETL are explored. The illustration of *f*-PSC with a planar heterojunction structure is depicted in Fig. 1(a). SnO_2-Au ETL is prepared via mixing the Au NPs with SnO_2 solution evenly, followed by spin coating and annealing (see the experimental section in detail). Figure 1(b) and the inset show the typical sample solutions of SnO_2 NPs, Au NPs, and 0.11 wt. % SnO_2-Au NPs in water, as well as their corresponding UV-vis absorption spectrum. Both Au NPs and 0.11 wt. % SnO_2-Au NPs exhibit a deep red color with a maximum absorption peak at 530 nm owing to the LSPR property of the Au NPs.[26]

The Au NPs are uniformly dispersed in the SnO_2 matrix with a diameter of approximately 20 nm [Fig. 1(c)]. The existence of small and uniform particles is beneficial for forming homogeneous and high-quality ETL thin film. The LSPR of plasmonic nanoparticles can enhance light absorption through either scattering into trapped optical

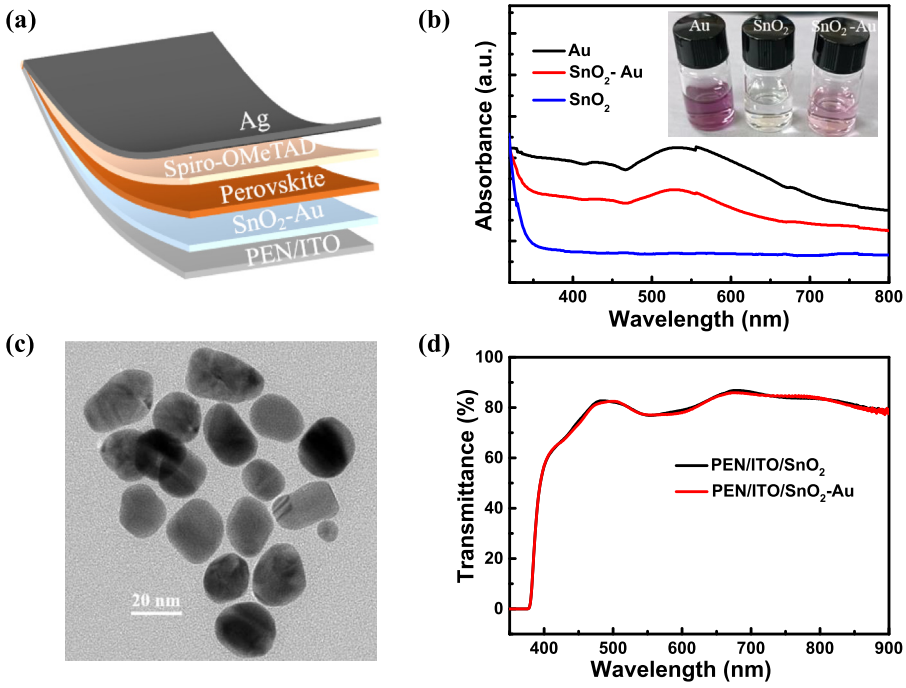

FIG. 1. (a) Schematic diagram of PSCs device architecture. (b) Absorption spectra of SnO_2, Au, and 0.11 wt. % SnO_2-Au NPs solutions, and insets show the photographs of three solutions. (c) TEM image of 0.11 wt. % SnO_2-Au NPs. (d) Transmittance spectra of PEN/ITO/SnO_2 and PEN/ITO/SnO_2-Au.

modes or by increasing the electromagnetic field near the particle.[19,25] Hence, the UV-vis transmittance spectra and absorption spectrum of different ETLs are detected to demonstrate the LSPR effect, as shown in Fig. 1(d) and Fig. S1. The 0.11 wt. % SnO_2-Au NPs thin film hardly changes in transmittance and absorption between 400 and 900 nm, which indicates that the Au NPs do not exhibit the LSPR characteristic in our case, perhaps due to the low concentration of Au NPs.

The top-view morphologies of SnO_2 and SnO_2-Au thin films are investigated using scanning electron microscopy (SEM) and atomic force microscope (AFM), as presented in Fig. S2, demonstrating that the morphology and roughness of SnO_2 thin film remain similar after embedding Au NPs. It is widely acknowledged that the substrate exerts a significant influence on the crystallization and growth of perovskite film.[27] Therefore, a stable SnO_2 morphology is very important to ensure the quality of upper perovskite film. Speculatively, the perovskite film deposited on SnO_2-Au ETL exhibits a comparable morphology and roughness with that on pristine SnO_2 ETL (Fig. S3 in the supplementary material), thereby facilitating the potential high performance of *f*-PSCs.

Furthermore, x-ray photoelectron spectroscopy (XPS) is performed to investigate the interactions between SnO_2 and Au NPs [Figs. S4(a) and S4(b) in the supplementary material]. The peaks corresponding to Sn 3d and O 1s in both SnO_2 and SnO_2-Au NPs show identical positions, suggesting the lack of any chemical bonding between Au NPs and SnO_2.[8] However, the absence of Au element is detected in all of the samples, primarily attributed to its ultra-low concentration. Moreover, the crystallization of SnO_2 and perovskite film almost does not change according to the x-ray diffraction pattern (XRD) [Figs. S4(c) and S4(d)].

As discussed above, small and uniform Au NPs are uniformly dispersed in the SnO_2 matrix without forming chemical bonds with SnO_2 [Fig. 1(c), Figs. S4(a) and S4(b) in the supplementary material]. Also, SnO_2-Au NPs thin film maintains the dense morphology, exhibits superior crystallization, and retains high transmittance as the same as pristine SnO_2 thin film, which is potentially beneficial for forming fancy perovskite films and devices [Fig. 1(d), Figs. S2 and S3 in the supplementary material]. Furthermore, SnO_2-Au NPs do not exhibit the LSPR characteristic in our case since low concentration of Au NPs [Fig. 1(d) and Fig. S1]. It is worth noting that the concentration of SnO_2 and SnO_2-Au NPs solutions is both 5%, while the 5% SnO_2-Au NPs solution is diluted from the 12% SnO_2 and 0.1 mg/ml Au NPs solutions (see the experimental section for details), resulting in a maximum concentration of Au NPs in SnO_2-Au NPs solutions of 0.11 wt. %.

It is expected that Au NPs can improve the charge transport and transfer properties of ETL. Accordingly, multiscale characterizations are conducted to investigate the electrical properties. For superior ETL in PSCs, efficient charge transport properties, such as high conductivity and mobility, are essential to achieve excellent performance parameters.[28–31] The conductivity of SnO_2 thin film is investigated according to the following equation:[28]

$$\sigma = \frac{Id}{VA}, \tag{1}$$

where A is the area (0.1 cm^2) of the device and d is the thickness (30 nm) of the thin film.[29] The $\frac{I}{V}$(14.2 and 48.6 mS for SnO_2 and SnO_2-Au thin film, respectively) is calculated from current–voltage (I-V) characteristic curves in Fig. 2(a). Therefore, the σ of SnO_2-Au thin film is calculated to be 1.46×10^{-3} mS cm^{-1}, which is three times higher than that of pure SnO_2 thin film (0.43×10^{-3} mS cm^{-1}).

Meanwhile, the devices with a structure of PEN/ITO/Au/ETL/Au are fabricated to calculate the electron mobilities of SnO_2 with or without Au NPs thin films by fitting the Mott–Gurney law, according to the following equation:[30]

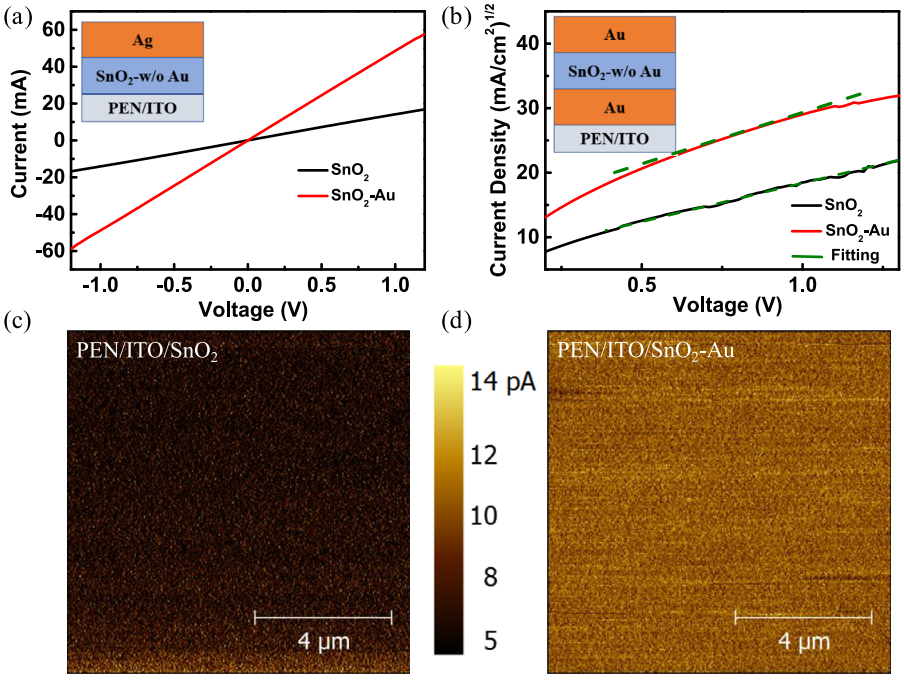

FIG. 2. (a) *I-V* curves of devices with the structure of PEN/ITO/ETL/Ag for calculating the conductivity of ETL. (b) Electron mobility for SnO_2 and 0.11 wt. % SnO_2-Au NPs thin films using the SCLC model, and the inset shows the device structure of PEN/ITO/Au/ETL/Au. The c-AFM images of (c) PEN/ITO/SnO_2 and (d) PEN/ITO/0.11 wt. % SnO_2-Au NPs thin films.

$$\mu_e = \frac{8JL^3}{9\varepsilon\varepsilon_0(V_{app} - V_r - V_{bi})^2}, \quad (2)$$

where J is the current density, ε_0 is the vacuum permittivity, ε is the dielectric permittivity of the rutile SnO_2 (9),[31] L is the thickness of the SnO_2 thin film (30 nm),[29] V_{app} is the applied voltage of the device, V_r is the voltage drop due to constant resistance and series resistance across the electrodes,[32] and V_{bi} is the built-in voltage due to the different work function of the two electrodes (here, $V_{bi} = V_r = 0$). The calculated mobilities are 3.36×10^{-3} and 8.45×10^{-3} $cm^2/V\,s$ for the SnO_2 and SnO_2-Au ETL, respectively [Fig. 2(b)], demonstrating that the Au NPs do effectively promote the electron transport.

Further, conductance atomic force microscopy (C-AFM) is carried out in order to observe the conductivity more intuitively. From the C-AFM results, the SnO_2-Au thin film shows significant higher average current of 14.5 pA than pristine SnO_2 thin film with an average current of 4.4 pA [Figs. 2(c), 2(d), and Fig. S5 in the supplementary material], which directly demonstrated that Au NPs could promote the conductivity of SnO_2 thin film. Moreover, the improvement for current is very uniform through the $10 \times 10\,\mu m^2$ area [Figs. 2(c), 2(d), and Fig. S5 in the supplementary material], meaning that the improvement is not localized only around near the Au NPs.

The improved electron mobility and conductivity of SnO_2-Au ETL can be attributed to the high electron mobility and electron conduction properties of tiny Au NPs. First, the small size (~20 nm) provides a larger specific surface area as compared to bulk gold materials, allowing Au NPs to have more conductive channels and resulting in increased conductivity.[33,34] Second, Au NPs exhibit unique electronic properties. Due to size restrictions, the electronic energy levels and lattice structure of Au NPs undergo changes. These changes can impede the mobility of electrons within the nanoparticles, leading to increased electron scattering and collision, thereby inducing electron localization. This electron localization enhances conductivity as electrons are able to effectively transfer during the scattering and transmission process within Au NPs.[35,36]

It is apparent that the high electron mobility can effectively facilitate electron transfer in PSCs, suppress carrier accumulation at the ETL/perovskite interface, and improve the PCEs.[37,38] A high conductive ETL possesses higher electron mobility and density, which is beneficial to promote charge transport and devices performance,[38,39] particularly in terms of the current density.[40] Moreover, the enhanced conductivity in SnO_2 thin film is expected to reduce series resistance (R_s) of devices, thereby potentially causing an increase in the fill factor (FF).[22,41]

The devices are fabricated with a structure of ITO/PEN/SnO_2 or SnO_2-Au NPs/perovskite/Spiro-OMeTAD/Ag. The efficient perovskite composition of $Rb_{0.02}FA_{0.98}PbI_{2.6}Cl_{0.4}$ with a bandgap of 1.525 eV was deposited through a two-step spin-coating process (Fig. S6 in the supplementary material). The different quantities of Au NPs solution were added to SnO_2, forming SnO_2-Au NPs ETL with different doping ratios (see the experimental section in detail). The corresponding performance is shown in Table S1. To further enhance the performance of *f*-PSC, a 2D/3D strategy is employed in control and 0.08%wt Au NPs devices.[6] The PCE histograms imply that SnO_2-Au NPs ETL obviously enhances efficiency and improves performance reproducibility as well [Fig. 3(a)], leading to an average PCE of 22.19% (Table S2, supplementary material). The champion *f*-PSC with pristine SnO_2 exhibits an optimized PCE of 21.65%, with a V_{oc} of 1.11 V, a J_{sc} of 24.51 mA/cm^2, and an *FF* of 79.6%. However, a champion *f*-PSC with SnO_2-Au NPs ETL achieves a inspiring PCE of 23.08% remarkably, with a V_{oc} of 1.13 V, a J_{sc} of 25.12 mA/cm^2, and an *FF* of 81.3%. The integrated photocurrent of SnO_2 and SnO_2-Au NPs ETL PSCs is calculated to be 24.0 and 24.5 mA/cm^2 stemmed from the external quantum efficiency (EQE) spectra [Fig. 3(c)], which are consistent with the results of *J-V*

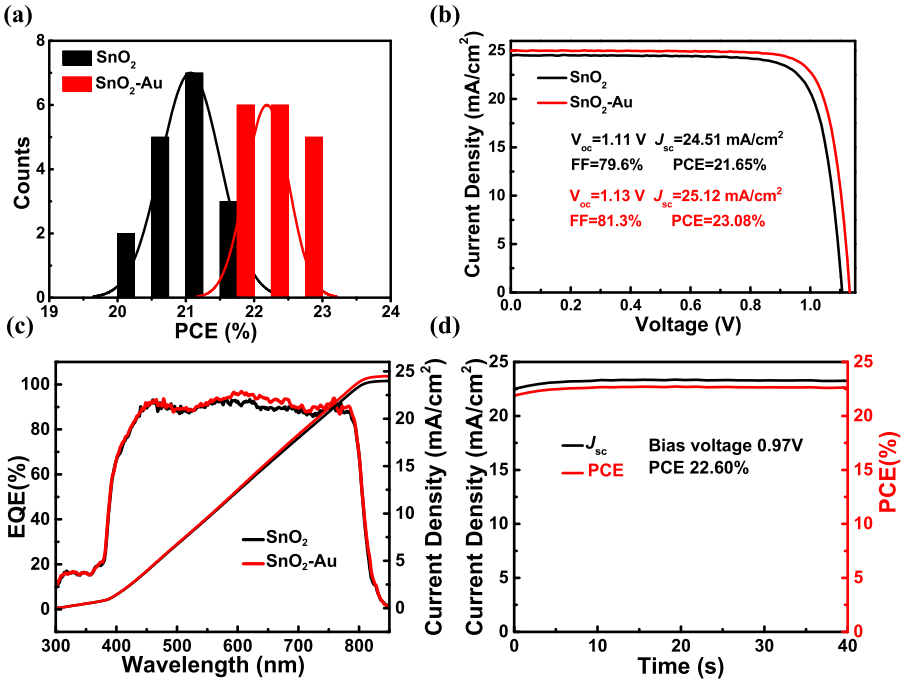

FIG. 3. (a) Histograms of PCEs for *f*-PSCs with SnO_2 and SnO_2-Au NPs ETL (reverse scanning, 0.02 V/s). (b) *J-V* curves of *f*-PSCs with SnO_2 and SnO_2-Au NPs ETL under 1 sun illumination (reverse scanning, 0.02 V/s). (c) External quantum efficiency (EQE) and corresponding integrated photocurrent. (d) The steady-state photocurrent and PCE for the champion device with SnO_2-Au NPs ETL at 0.97 V bias under 1 sun illumination.

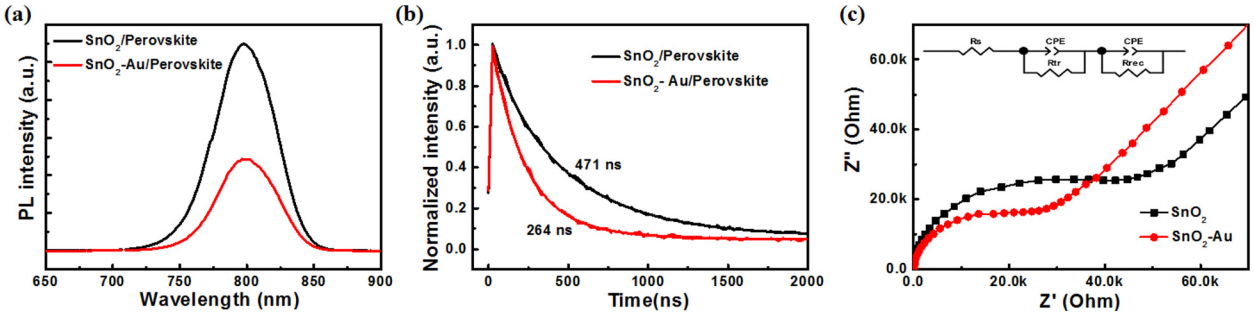

FIG. 4. (a) The steady state and (b) time-resolved PL for SnO_2/perovskite and SnO_2-Au/perovskite, respectively. (c) EIS plots for SnO_2 and SnO_2-Au ETL devices. The devices were tested without bias voltage in an atmospheric environment with a humidity of ~40%. The inset shows the equivalent circuit.

measurements. Figure 3(d) shows the stabilized power output at the maximum power point (MPP) for SnO_2-Au NPs ETL device under AM 1.5 G illumination at a bias voltage of 0.97 V. A stabilized PCE of 22.60% is achieved, indicating that SnO_2-Au NPs ETL device holds a stable output. The enhancement of device performance is owed to the remarkable electric properties of SnO_2-Au NPs ETL with superior electron mobility and conductivity, which enhance charge transport and decrease charge recombination at the ETL/perovskite interface. A cross section SEM is used to measure the thickness of flexible substrates, as shown in Fig. S7. The substrate has a thickness of approximately 135 μm. It is worth noting that the incorporation of Au NPs has no positive effect on the bending performance of *f*-PSCs (Fig. S8 in the supplementary material).

For exploring the charge carrier dynamics in PSCs using SnO_2 ETL with or without Au NPs, steady photoluminescence (PL) spectroscopy is carried out. As shown in Fig. 4(a), the SnO_2-Au NPs ETL shows a diminished PL intensity, suggesting a more efficient charge extraction in PSCs with SnO_2-Au ETL. In addition, the time-resolved PL (TRPL) spectroscopy [Fig. 4(b)] reveals more information about the charge dynamic process, which is fitted with a bi-exponential decay function (Table S3, supplementary material). τ_{avg} decreases from 471 ns to 264 ns for the perovskite films on SnO_2 and SnO_2-Au NPs ETL, meaning a more effective electron transfer from the perovskite to SnO_2-Au NPs ETL.

Afterward, electrochemical impedance spectroscopy (EIS) characteristics for *f*-PSCs with SnO_2 and SnO_2-Au NPs ETL are carried out under dark condition [Fig. 4(c)]. The fitted equivalent circuit model consists of series resistance (R_s) internally the perovskite films, and charge transfer resistance (R_{tr}) and recombination resistance (R_{rec}) at the interfaces constituting a parallel circuit with capacitor.[42–45] The fitted parameters are summarized in Table S4. The similar R_{rec} and R_s for different devices reveal that the Au NPs do not affect the internal properties of perovskite film. However, R_{tr} for SnO_2 and SnO_2-Au NPs device is decreased from 55 379 to 37 425 Ω, indicating the elevated extraction/transport at perovskite/SnO_2-Au NPs interfaces. These results are in accord with the aforementioned analyses of conductivity and mobilities and further demonstrate the enhanced electron extraction and transport properties of the SnO_2-Au NPs ETL, which are responsible for the superior performance of SnO_2-Au NPs devices.

In summary, we present a straightforward approach by embedding Au NPs in SnO_2 ETL to enhance the efficiency of *f*-PSCs. Such optimization approach results in remarkable improvement of electron mobilities, conductivity, and electron extraction capacity in SnO_2 ETL, while simultaneously reducing the charge carrier recombination in perovskite/SnO_2-Au interfaces. Therefore, a champion *f*-PSC achieves a PCE of 23.08% with a V_{oc} of 1.13 V, a J_{sc} of 25.12 mA/cm^2, and a *FF* of 81.3%. Our work outlines a facile method to fabricate high-efficiency *f*-PSCs by enhancing charge transport properties, which is compatible with industrial manufacturing of *f*-PSCs.

See the supplementary material for more data and data analysis on relevant experiment results.

This work was supported by the National Key Research and Development Program of China (No. 2022YFB3803300), the National Natural Science Foundation of China (Nos. 52173192 and 52203250), and China Postdoctoral Science Foundation (No. 2022TQ0375).

AUTHOR DECLARATIONS

Conflict of Interest

The authors have no conflicts to disclose.

Author Contributions

Caoyu Long: Conceptualization (equal); Data curation (equal); Formal analysis (equal); Investigation (equal); Writing – original draft (equal). **Erming Feng:** Formal analysis (supporting); Methodology (supporting). **Jianhui Chang:** Formal analysis (supporting); Methodology (supporting). **Yang Ding:** Data curation (supporting); Methodology (supporting). **Yuanji Gao:** Investigation (supporting); Methodology (supporting). **Hengyue Li:** Formal analysis (equal); Funding acquisition (equal); Writing – review & editing (equal). **Biao Liu:** Methodology (supporting). **Zijian Zheng:** Methodology (supporting); Writing – review & editing (supporting). **Liming Ding:** Methodology (supporting); Writing – review & editing (supporting). **Junliang Yang:** Formal analysis (equal); Funding acquisition (equal); Methodology (equal); Supervision (equal); Writing – review & editing (equal).

DATA AVAILABILITY

The data that support the findings of this study are available from the corresponding authors upon reasonable request.

REFERENCES

[1]S. D. Stranks, G. E. Eperon, G. Grancini, C. Menelaou, M. J. Alcocer, T. Leijtens, L. M. Herz, A. Petrozza, and H. J. Snaith, Science **342**(6156), 341–344 (2013).
[2]X. X. Feng, B. Liu, Y. Y. Peng, C. Gu, M. Q. Long, M. Q. Cai, C. J. Tong, L. Y. Han, and J. L. Yang, Small **18**(22), 2201831 (2022).
[3]See https://www.nrel.gov/pv/assets/pdfs/best-research-cell-efficiencies.20230726.pdf for "Efficiency chart."
[4]B. Han, Y. H. Wang, C. Liu, K. X. Sun, M. J. Yang, L. S. Xie, S. C. Yang, Y. Y. Meng, S. Y. Lin, P. Xu, J. Li, Q. Q. Qiu, and Z. Y. Ge, Angew. Chem. Int. Ed. **62**(8), e202217526 (2023).
[5]M. Li, J. Zhou, L. Tan, H. Li, Y. Liu, C. Jiang, Y. Ye, L. Ding, W. Tress, and C. Yi, Innovation **3**(6), 100310 (2022).
[6]D. Gao, B. Li, Z. Li, X. Wu, S. Zhang, D. Zhao, X. Jiang, C. Zhang, Y. Wang, Z. Li, N. Li, S. Xiao, W. C. H. Choy, A. K. Y. Jen, S. Yang, and Z. Zhu, Adv. Mater. **35**(3), 2206387 (2023).
[7]X. X. Wu, G. Y. Xu, F. Yang, W. J. Chen, H. Y. Yang, Y. X. Shen, Y. Y. Wu, H. Y. Chen, J. C. Xi, X. H. Tang, Q. R. Cheng, Y. J. Chen, X. M. Ou, Y. W. Li, and Y. F. Li, ACS Energy Lett. **8**(9), 3750–3759 (2023).
[8]Z. Y. Chen, Q. R. Cheng, H. Y. Chen, Y. Y. Wu, J. Y. Ding, X. X. Wu, H. Y. Yang, H. Liu, W. J. Chen, X. H. Tang, X. H. Lu, Y. W. Li, and Y. F. Li, Adv. Mater. **35**(18), 2300513 (2023).
[9]Y. H. Wang, Y. Y. Meng, C. Liu, R. K. Cao, B. Han, L. S. Xie, R. J. Tian, X. Y. Lu, Z. H. Song, J. Li, S. C. Yang, C. D. Lu, and Z. Y. Ge, Joule (published online 2024).
[10]Z. H. Zheng, F. M. Li, J. Gong, Y. Y. Ma, J. W. Gu, X. C. Liu, S. H. Chen, and M. Z. Liu, Adv. Mater. **34**(21), 2109879 (2022).
[11]D. Yang, R. Yang, K. Wang, C. Wu, X. Zhu, J. Feng, X. Ren, G. Fang, S. Priya, and S. Liu, Nat. Commun. **9**(1), 3239 (2018).
[12]Z. Liu, K. Deng, J. Hu, and L. Li, Angew. Chem. Int. Ed. **131**(33), 11621–11628 (2019).
[13]D. Liu, Y. Wang, H. Xu, H. Zheng, T. Zhang, P. Zhang, F. Wang, J. Wu, Z. Wang, Z. Chen, and S. Li, Sol. RRL **3**(2), 1800292 (2019).
[14]P. Zhu, S. Gu, X. Luo, Y. Gao, S. Li, J. Zhu, and H. Tan, Adv. Energy Mater. **10**(3), 1903083 (2020).
[15]W. Hui, Y. Yang, Q. Xu, H. Gu, S. Feng, Z. Su, M. Zhang, J. Wang, X. Li, J. Fang, F. Xia, Y. Xia, Y. Chen, X. Gao, and W. Huang, Adv. Mater. **32**(4), 1906374 (2020).
[16]E. H. Jung, B. Chen, K. Bertens, M. Vafaie, S. Teale, A. Proppe, Y. Hou, T. Zhu, C. Zheng, and E. H. Sargent, ACS Energy Lett. **5**(9), 2796–2801 (2020).
[17]J. Zhuang, P. Mao, Y. Luan, N. Chen, X. Cao, G. Niu, F. Jia, F. Wang, S. Cao, and J. Wang, Adv. Funct. Mater. **31**(17), 2010385 (2021).
[18]Y. J. Gao, X. X. Feng, J. H. Chang, C. Y. Long, Y. Ding, H. Y. Li, K. Q. Huang, B. Liu, and J. L. Yang, Appl. Phys. Lett. **121**(7), 073902 (2022).
[19]S. S. Mali, S. H. Chang, and K. H. Chang, Nanoscale **8**(5), 2664–2677 (2016).
[20]D. S. Lee, W. J. Kim, B. G. Cha, J. Kwon, S. J. Kim, M. Kim, J. Y. Kim, D. H. Wang, and J. H. Park, ACS Appl. Mater. Interfaces **8**(1), 449–454 (2016).
[21]C. X. Zhang, C. X. Luo, Q. Shi, J. H. Yue, L. Y. Wang, Z. B. Chen, X. H. Huang, and S. Mei, Nanoscale **9**(8), 2852–2864 (2017).
[22]S. A. Xiao, F. Xu, Y. Bai, J. Y. Xiao, T. Zhang, C. Hu, X. Y. Meng, H. R. Tan, H.-P. Ho, and S. H. Yang, Sol. RRL **3**(2), 1800278 (2019).
[23]Tulus, S. Olthof, M. Marszalek, A. Peukert, L. A. Muscarella, B. Ehrler, O. Vukovic, Y. L. Galagan, S. C. Boehme, and E. von Hauff, ACS Appl. Energy Mater. **2**(5), 3736–3748 (2019).
[24]D. W. Zhao, M. Y. Yu, L. L. Zheng, M. Li, S. J. Dai, D. C. Chen, T. C. Lee, and D. Q. Yun, ACS Appl. Energy Mater. **3**(10), 9568–9575 (2020).
[25]D. M. Zheng, C. Schwob, Y. Prado, Z. Ouzit, L. Coolen, and T. Pauporté, Nano Energy **94**, 106934 (2022).
[26]K. M. Mayer and J. H. Hafner, Chem. Rev. **111**(6), 3828–3857 (2011).
[27]Y. G. Yang, H. Z. Lu, S. L. Feng, L. F. Yang, H. Dong, J. Wang, C. Tian, L. Li, H. L. Lu, J. K. Jeong, S. M. Zakeeruddin, Y. H. Liu, M. Gratzel, and A. Hagfeldt, Energy Environ. Sci. **14**(6), 3447–3454 (2021).
[28]J. H. Heo, M. S. You, M. H. Chang, W. Yin, T. K. Ahn, S.-J. Lee, S.-J. Sung, D. H. Kim, and S. H. Im, Nano Energy **15**, 530–539 (2015).
[29]K. Q. Huang, Y. Y. Peng, Y. X. Gao, J. Shi, H. Y. Li, X. D. Mo, H. Huang, Y. L. Gao, L. M. Ding, and J. L. Yang, Adv. Energy Mater. **9**(44), 1901419 (2019).
[30]D. Yang, X. Zhou, R. X. Yang, Z. Yang, W. Yu, X. L. Wang, C. Li, S. Z. (Frank) Liu, and R. P. H. Chang, Energy Environ. Sci. **9**(10), 3071–3078 (2016).
[31]K. Q. Huang, X. X. Feng, H. Y. Li, C. Y. Long, Y. L. Gao, Q. B. Meng, K. Weber, T. Duong, and J. L. Yang, Adv. Sci. **9**(35), 2204163 (2022).
[32]S. Park, J. H. Heo, C. H. Cheon, H. Kim, S. H. Im, and H. J. Son, J. Mater. Chem. A. **3**(48), 24215–24220 (2015).
[33]X. S. Liu, H. Li, Q. Jin, and J. Ji, Small **10**(21), 4230–4242 (2014).
[34]J. Y. Chen, F. Saeki, B. J. Wiley, H. Cang, M. J. Cobb, Z-Y. Li, L. Au, H. Zhang, M. B. Kimmey, X. D. Li, and Y. N. Xia, Nano Lett. **5**(3), 473–477 (2005).
[35]A. Hoggard, L. Y. Wang, L. Ma, Y. Fang, G. You, J. Olson, Z. Liu, W. S. Chang, P. M. Ajayan, and S. Link, ACS Nano **7**(12), 11209–11217 (2013).
[36]C. C. Huang, Z. Yang, K. H. Lee, and H. T. Chang, Angew. Chem. **119**(36), 6948–6952 (2007).
[37]Q. Jiang, L. Q. Zhang, H. L. Wang, X. L. Yang, J. H. Meng, H. Liu, Z. G. Yin, J. L. Wu, X. W. Zhang, and J. B. You, Nat. Energy **2**(1), 16177 (2016).
[38]H. Y. Li, X. X. Feng, K. Q. Huang, S. Y. Lu, X. Y. Wang, E. M. Feng, J. H. Chang, C. Y. Long, Y. J. Gao, Z. H. Chen, C. Y. Yi, J. He, and J. L. Yang, Small **19**(24), 2300374 (2023).
[39]R. H. Yuan, B. Cai, Y. H. Lv, X. Gao, J. W. Gu, Z. H. Fan, X. H. Liu, C. Yang, M. Z. Liu, and W. H. Zhang, Energy Environ. Sci. **14**(9), 5074–5083 (2021).
[40]H. Wang, X. Zhang, F. Gong, G. Zhou, and Z. S. Wang, Adv. Mater. **24**(1), 121–124 (2012).
[41]S. D. Stranks and H. J. Snaith, Nat. Nanotechnol. **10**(5), 391–402 (2015).
[42]A. Guerrero, G. G. Belmonte, I. M. Sero, J. Bisquert, Y. S. Kang, T. J. Jacobsson, J. P. C. Baena, and A. Hagfeldt, J. Phys. Chem. C **120**(15), 8023–8032 (2016).
[43]C. Yang, Z. Wang, Y. Lv, R. Yuan, Y. Wu, and W. H. Zhang, Chem. Eng. J. **406**, 126855 (2011).
[44]K. Q. Huang, H. Y. Li, C. J. Zhang, Y. X. Gao, T. J. Liu, J. Zhang, Y. L. Gao, Y. Y. Peng, L. M. Ding, and J. L. Yang, Sol. RRL **3**(3), 1800318 (2019).
[45]Y. Zhao, F. Ma, Z. H. Qu, S. Q. Yu, T. Shen, H. X. Deng, X. B. Chu, X. X. Peng, Y. B. Yuan, X. W. Zhang, and J. B. You, Science **377**(6605), 531–534 (2022).